Theor Chem Acc (2012) 131:1107
DOI 10.1007/s00214-012-1107-0

REGULAR ARTICLE

Ruthenium(II) complexes with new large-surface ligands based on electron-accepting expanded pyridiniums: insights from density functional theory

Samira Zeroual · Nathalie Bouet · Fabien Tuyèras · Cyril Peltier · Nadia Ouddai · Philippe Ochsenbein · Carlo Adamo · Philippe P. Lainé · Ilaria Ciofini

Received: 8 July 2011 / Accepted: 17 September 2011 / Published online: 8 February 2012

Abstract With the aim of designing new inorganic photosensitizers for photovoltaic applications, the structural and electronic properties of two Ru(II) complexes containing terpyridine-based ligands derived from expanded pyridiniums both branched—polyphenyl—and fused—polycyclic—were investigated by the means of density functional theory (DFT) and time-dependent DFT (TD-DFT). In particular, the structure and electronic absorption of the fused architectures—including the isolated ligand and its complex—were compared with those of their respective branched precursors with the aim to account for the their enhanced electronic features in the visible spectral region. The theoretical insights gained into the "large-surface" ligand and its associated complex open the route for a joint experimental and theoretical design of new inorganic photosensitizers based on fused expanded pyridiniums.

Keywords DFT · TD-DFT · Ruthenium(II) complexes · Expanded pyridinium acceptors

Electronic supplementary material The online version of this article (doi:10.1007/s00214-012-1107-0) contains supplementary material, which is available to authorized users.

S. Zeroual · N. Bouet · C. Peltier · C. Adamo · I. Ciofini (✉)
LECIME, Laboratoire d'Électrochimie, Chimie des Interfaces et Modélisation pour l'Énergie, UMR 7575 CNRS, École Nationale Supérieure de Chimie de Paris – Chimie ParisTech,
11 rue P. et M. Curie, 75231 Paris Cedex 05, France
e-mail: ilaria-ciofini@chimie-paristech.fr

S. Zeroual · N. Ouddai
Laboratoire de chimie de materiaux et des vivants: Activité, Réactivité, Université de Batna, 05000 Batna, Algeria

F. Tuyèras · P. P. Lainé (✉)
Laboratoire ITODYS, UMR 7086 CNRS, Université Paris Diderot, Sorbonne Paris Cité, Bâtiment Lavoisier,
15, rue Jean-Antoine de Baïf, 75205 Paris Cedex 13, France
e-mail: philippe.laine@univ-paris-diderot.fr

P. Ochsenbein
Laboratoire de Cristallographie et Modélisation Moléculaire du Solide, Sanofi-Aventis LGCR, 371 rue du Professeur Blayac,
34184 Montpellier Cedex 04, France

1 Introduction

The last decades have witnessed an increasing interest from the community of chemists toward the conception and modeling of functional (supra-) molecular assemblies able to perform, in a controlled fashion, light-driven acts. These light-triggered phenomena span from mere photoinduced charge-separation (Artificial Photosynthesis) or charge injection (Photovoltaics) to more sophisticated transduction processes encountered in photochemical molecular devices (PMDs), as in the instance of molecular machines powered by light [1]. The scope of the present work lies in the first category of basic photoactive assemblies meant to play a role in solar energy conversion. More specifically, the aim is to design redox-active photosensitizers whose spectral activity would ideally encompass the whole visible plus NIR domain, that is, panchromatic dyes also colloquially referred to as black absorbers. In the field of such purposely conceived compounds, restricting the scope to inorganic species, adopted synthetic strategies are essentially three [2]:

- Approach 1: manipulating features of specific metal-to-ligand charge-transfer (MLCT) characteristics by changing (i) peripheral substituents of organic ligands and/or (ii) the nature of ancillary ligands and/or (iii) the nature of metal ion(s) [3–5];

- Approach 2: assembling different types of inorganic chromophores so as to build antenna systems [6, 7] and to possibly covering the whole visible region [8];
- Approach 3: using so-called large-surface ligands [9], that is, organic ligands having extended π-conjugated systems to generate low-energy and broad MLCT absorption band(s) [8, 10–12]. This less commonly adopted approach is the one explored in the present study.

In a nowadays classic fashion to produce directional photoinduced electron transfers, a redox-active photosensitizer (P) is covalently linked to an electron acceptor (A) in such a manner that upon light excitation in the visible region, an excited state of the $[P^+–A^-]^*$ type is formed. When dealing with genuine charge-separated (CS) states, long-lived excited states are targeted. They are obtained by arranging conveniently weak electronic coupling between the functional units to reduce the efficiency of adverse and competing charge recombination (i.e., fast backward electron transfer to the P-A ground state). Because the tuning and characterization of the electronic coupling at both the ground and the excited states are often experimentally (including synthetically) challenging, it is not surprising that several recent works integrating theoretical and experimental approaches are specifically focused on this crucial point to enhance the properties of new PMDs [13–16]. Regarding the inorganic photosensitizers involved in dye-sensitized solar cells (DSSCs), these are chromophores usually displaying huge—and possibly long-range—MLCT states rather than genuine CS states [17–20]. The lifetime of the $[P^+–A^-]^*$ states is not a critical parameter since charge injection into semiconductors can occur from "hot" (i.e., non-relaxed) excited states, at the subpicosecond timescale [21]. Thereby, the fine-tuning of the intercomponent electronic coupling is no longer a key matter for the design. Closely coupled and structurally compact assemblies embodied in made-in-one-piece structural units, however, hosting separate—functional—electronic entities (P and A) can therefore be envisioned. Benchmark examples of such peculiar compounds are given by Ru(II)/Os(II) complexes of polycyclic aromatic dppz [22] and similar ligands [23].

In this work, we concentrate on dyads (Fig. 1) made up of a ruthenium(II)-bis terpyridine complex as the photosensitizer (denoted as **P**) and of a covalently linked pyridinium-based moiety fulfilling the function of the electron acceptor (denoted as **A**). The two following types of **A** groups are more specifically involved: 1,2,4,6-tetraarylpyridiniums and their bis-cyclized derivatives, referred to as *branched* (**Ab**) and *fused* (**Af**) expanded pyridiniums, respectively (see Fig. 1). These expanded pyridiniums have been selected because the impact of the extension of the π system of pyridiniums on their redox, electronic, and photophysical properties has been recently established in details by some of us [24–27]. Affiliated 2,2′:6′,2″-terpyridine (tpy) ligands (**L**) bearing these acceptors are denoted as **L-Ab** (the pyridinium ring is linked to the tpy via a single covalent bond) and **LAf** (the pyridinium ring is embedded within the fused polycyclic and made-in-one-piece "large-surface" ligand). Similarly, related heteroleptic complexes (i.e., dyads) are denoted **P-Ab** and **PAf** (Fig. 1). In the present study, the **P-Ab** compound serves as a reference to assess the contribution of the extension of the π-conjugated system in the electronic properties of the fused analog **PAf**.

The structural and electronic properties of the isolated ligands (**L-Ab** and **LAf**) as well as those of the dyads (**P-Ab** and **PAf**) were investigated by the means of density functional theory (DFT). Vertical excited states (that is, absorption spectra) were computed at time-dependent DFT level (TD-DFT). Several previous works have already pointed out the very good performances of DFT and TD-DFT in the description and prediction of ground and excited state properties of both organic and inorganic systems, especially when using hybrid exchange correlation functionals and properly including solvent effects (see for instance [28, 29] and references therein). Nonetheless, some failures of DFT and TD-DFT are also nowadays quite well established and, in particular, it is recognized that even when using hybrid functionals, a particular care should be taken when dealing with charge-transfer excitations in the case of a real through space electron transfer [30]. Specific diagnostic indexes of eventual pathological cases have also been developed in this framework [31, 32].

The paper is structured as follows. After a brief recall of the computational approaches used (Sect. 2), the geometrical and electronic structures of the ligands and the dyads are discussed in Sect. 3. Next, the photophysical properties of all systems are collected in Sect. 4, while the final section is devoted to the general conclusions and perspectives including a discussion on the chemical feasibility of the systems herein proposed.

2 Computational details

All calculations were carried out with the Gaussian09 code [33]. A hybrid Hartree–Fock/density functional model, referred to as PBE0, was used [34]. This functional has been chosen as it has recently been proven to yield reliable excitations in organic dyes not only for valence transitions but also for excitations with charge-transfer character, provided that a sufficient orbital overlap is present [28, 29].

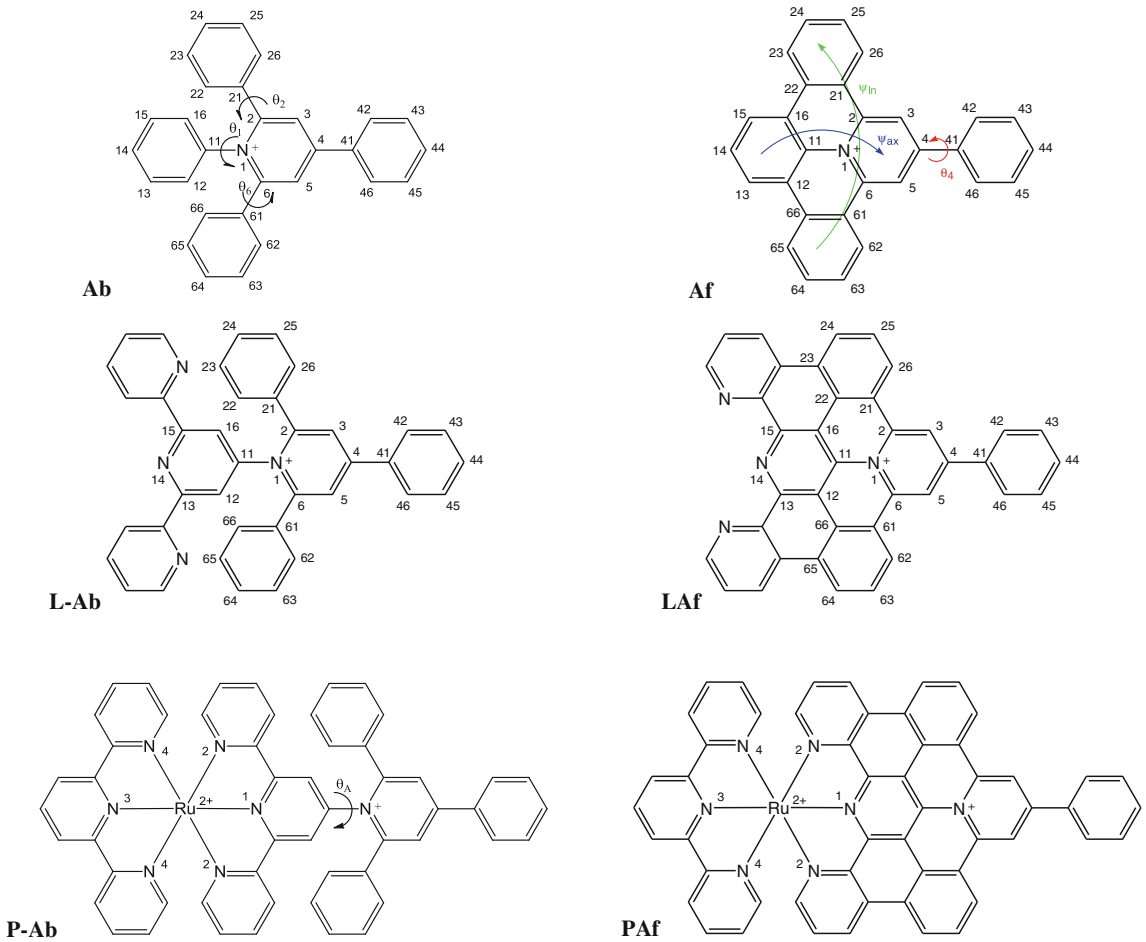

Fig. 1 Schematic drawing and labeling scheme of the ligands studied in this work (**L-Ab** and **LAf**) together with the corresponding parent acceptors (**Ab** and **Af**) and dyads (**P-Ab** and **PAf**)

Unless otherwise specified, structural optimizations and subsequent frequency calculations for the ground state were performed, in the gas phase, using an all electron double zeta basis set (LANL2) and corresponding pseudopotential in the case of the Ru atom. Vertical excitations were computed by the means of TD-DFT at the same level of theory. When bulk solvent effects were included, the Polarizable Continuum Model (PCM) of Tomasi and co-workers was applied [35]. More specifically, the conductor-like PCM model as implemented in Gaussian (CPCM) [36] was applied, and acetonitrile (CH_3CN) was considered as solvent because of its common experimental use for the type of molecules herein studied.

3 Structural and electronic features

The geometrical and electronic properties of the parent acceptors **Ab** and **Af** at both the ground and the excited states were recently studied [24–27]. The main geometrical parameters, computed for the ground state of molecules **L-Ab** and **LAf** in the gas phase, are reported in Table 1 along with experimental data available for **L-Ab** and the corresponding parameters computed for **Ab** and **Af**. The labeling Scheme used is given in Fig. 1.

In order to clarify the effect of the phenyl substituent at the position 4 of the pyridinium ring, two additional ligands (**L-Ab^{H}** and **LAf^{H}**, Figure SI.1) lacking this phenyl terminus but having instead a hydrogen atom were also studied. Since the structural differences between the parent and the hydrogen substituted ligands are only marginal, all the conclusions drawn for **L-Ab** and **LAf** also hold for **L-Ab^{H}** and **LAf^{H}** and, for this reason, their structures are given only as Supporting Information (Table SI.1).

In the case of the branched ligands (**L-Ab** and **L-Ab^{H}**), the most stable—trans—conformation of the tpy unit was considered. First, a good agreement between available experimental data [37] and the computed outcomes can be noted. The largest deviation with respect to the X-ray data [37] is, in fact, of only ca. 0.033 Å in bond lengths and of ca. 5° for the most significant dihedral angles, if one puts aside the inaccuracy on the θ_6 value (of ca. 14.8°) mainly

Table 1 Main structural parameters (distance in Å, angles in degrees) computed for the relaxed geometries of **L-Ab** and **LAf**

	L-Ab	**Ab**		**LAf**	**Af**
N_1C_2	1.384	1.381 (1.369)	N_1C_2	1.405	1.404 (1.399)
C_2C_3	1.391	1.391 (1.371)	C_2C_3	1.393	1.393 (1.381)
C_3C_4	1.410	1.408 (1.399)	C_3C_4	1.401	1.398 (1.386)
C_4C_5	1.410	1.408 (1.394)	C_4C_5	1.401	1.398 (1.386)
C_5C_6	1.391	1.391 (1.368)	C_5C_6	1.393	1.393 (1.381)
C_6N_1	1.384	1.381 (1.374)	C_6N_1	1.405	1.404 (1.399)
N_1C_{11}	1.462	1.462 (1.466)	N_1C_{11}	1.421	1.428 (1.433)
C_2C_{21}	1.482	1.484 (1.488)	C_2C_{21}	1.461	1.460 (1.456)
C_4C_{41}	1.472	1.475 (1.475)	C_4C_{41}	1.473	1.476 (1.480)
C_6C_{61}	1.482	1.484 (1.479)	C_6C_{61}	1.461	1.460 (1.455)
θ_1	70.7	70.4 (78.6)	θ_1	–	–
θ_2	59.0	60.7 (55.9)	θ_2	–	–
θ_4	28.4	28.0 (25.1)	θ_4	32.0	30.0 (34.4)
θ_6	55.3	57.2 (71.8)	θ_6	–	–
			ψ_{ax}^{a}	179.3	179.8 (178.9)
			ψ_{ln}^{b}	179.8	179.8 (178.6)

Available X-ray data [25, 37] are reported in parenthesis while data computed in CH_3CN for systems **Ab** and **Af** are taken from Ref. [26]. Refer to Fig. 1 for labeling scheme

[a] ψ_{ax} corresponds to the $C_6N_1C_{11}C_{16}$ dihedral angle

[b] ψ_{ln} corresponds to the $N_1C_2C_{21}C_{26}$ dihedral angle. X-ray data from Ref. [25]

ascribable to the presence of nearby counterion and solvent molecule in the X-ray structure as well as to crystal packing [see cif file in ref. 37]. Determining properly the value of the intercomponent twist angle (θ_1) is of importance for such compact semirigid and potentially fully conjugate systems since this structural parameter not only governs the intramolecular electronic coupling [37–39] but is also likely to impact on electronic properties.

In general, in the case of the branched systems, tilt angles with respect to the central pyridinium ring of ca. 60° are computed for the phenyls at positions 2 and 6 while the pyridine ring (of tpy) connected at position 1 of the pyridinium is found more orthogonal by ca. 10° ($\theta_1 = 70.7°$). These values well compare with the X-ray data and, in particular, for the large θ_1 value measured (78.6°).

This large geometrical decoupling is straightforwardly ascribed to intramolecular steric hindrance between vicinal aryl rings connected to the pyridinium platform, that is, the pyridine ring (of tpy) at the position 1 and phenyl groups at positions 2/6 [37]. It remains nonetheless that a non-negligible electronic coupling of the acceptor unit with the photosensitizer is expected since the two moieties are geometrically not fully decoupled (that is, θ_1 is not 90°) [13–16].

Furthermore, the torsional motions responsible for the planarization of the phenyl and pyridine substituents are expected to be associated with soft (i.e., low energy) vibrational modes at both the ground and the excited states. In particular, the computed vibrational frequencies associated with interannular conformational changes leading to planarization are computed to be 43 and 46 cm^{-1} for **L-Ab**, very close to the values recently computed for the parent acceptor, **Ab** (that is, 38 and 21 cm^{-1} [26]).

Concerning the structure of fused molecules in general, no significant change in bond lengths of the pyridinium core is found compared to the branched analog excepted for the contraction (of ca. 0.04 Å) of the C_{11}–N^+ bond as a result of its partial double-bond character in the fused architectures.

Interestingly, it is worth noting that while the calculations predict a slightly non-planar molecular scaffold at the ground and at the excited state, as for the fused acceptor unit (**Af**), the fully fused "large-surface" ligand (**LAf**) shows a perfectly planar skeleton. This planarity is therefore to be ascribed to steric constrains induced by the full cyclization rather than to some intrinsic properties of the acceptor unit, in agreement with previous results on fused acceptors [24–26, 40]. Clearly, **LAf** is by construction characterized by a full electronic and geometrical coupling between the tpy moiety and the acceptor units, which are fused to giving rise to an overall π-conjugated/extended system.

The different degree of geometrical (de-)coupling computed for **L-Ab** and **LAf** sizably impacts the electronic structures of these systems. Typically, when the tpy and pyridinium moieties are only weakly coupled, as is the case for **L-Ab**, the highest occupied molecular orbital HOMO (of π character) and HOMO-1 (n character) are roughly degenerate and centered exclusively on the tpy unit (Figure SI.2) while the LUMO (lowest unoccupied molecular orbital) and LUMO+1 are essentially located on the pyridinium ring (Figure SI.2). Regarding **LAf**, it is worth noting that the shape (i.e., spatial expanse and character) of the frontiers orbitals (from HOMO-1 to LUMO+1) is roughly the same as for **L-Ab**. Nevertheless, a significant change in the orbital ordering can be noticed, the main

Table 2 Main structural parameters (distance in Å, angles in degrees) computed for the relaxed geometries of **P-Ab** and **PAf**

	P-Ab	PAf
Ru-N_1	1.983 (1.986)	1.967
Ru-N_2	2.080/2.080 (2.085/2.085)	2.146/2.146
N_2-N_1-N_2	104.0 (104.1)	108.4
Ru-N_3	2.000 (1.981)	2.003
Ru-N_4	2.085/2.085 (2.096/2.079)	2.087/2.087
θ_A	68.4 (80.7)	0.3

Refer to Fig. 2 for labeling scheme. X-ray data (from Ref. [37]) are reported in parenthesis

difference stemming in the n character of the HOMO in the case of **LAf**.

Overall, the impact of structural fusion of the ligand **L-Ab** into its **LAf** counterpart results in a densification of states in the immediate vicinity of the HOMO–LUMO gap involving both virtual and filled MOs. Nevertheless, frontier orbitals are not sizably affected by the extension of the pi-conjugated system, which essentially alters MOs other than the HOMO-1 to LUMO+1 orbitals in **LAf** (Figure SI.2). In other words, electronic absorption is expected to increase and extend toward lower energies in the case of the fused compound.

To some extent, these combined features (i.e., made-in-one-piece structure but spatially separate electronic functions) are reminiscent of that of above-mentioned dppz ligand and complexes [22].

As regards inorganic dyads **P-Ab** and **PAf**, the most relevant geometrical parameters computed in the gas phase are reported in Table 2. The numbering scheme used is given in Fig. 1 while data related to the optimized ground state structures are collected in Fig. 2. Again, since structural effects associated with the substitution of the phenyl at position 4 of the pyridinium ring with a hydrogen atom are marginal, all the conclusions drawn for **P-Ab** and **PAf** also hold for **P-Ab^{H}** and **PAf^{H}**, whose structural features are given as Supporting Information (Table SI.2).

A general good agreement between the computed structure and the structure obtained by single-crystal X-ray diffraction is found in the case of **P-Ab**. In particular, the coordination sphere of the ruthenium(II) metal cation is very well reproduced, the maximal error in Ru–N distances being of only 0.019 Å. The geometrical decoupling between **P** and **Ab** ruled by θ_A, that is, the torsional angle between the planes of pyridinium and tpy, seems on the other hand slightly overestimated by the calculations. However, one can reasonably consider that the level of theory here applied is able to correctly reproduce the structural features of the dyads, thereby allowing the safe comparison of the results obtained for **P-Ab** and **PAf**.

Focusing on the ruthenium coordination sphere, it is worth noticing that while the Ru-N_1 distances computed for **P-Ab** and **PAf** are comparable, the Ru-N_2 distances are significantly larger (by ca. 0.064 Å) in the case of the complex containing the fused ligand, that is, for **PAf**.

This finding is related to the different degree of flexibility of the two ligands. In fact, while the **L-Ab** ligand can easily rearrange in order to properly coordinate the Ru atom via the closure of the N_2–N_1–N_2 bite angle that reduces to 104°, this angle is constrained to a larger value (of ca. 108°) with consequent increase in the Ru–N_2 distances in the case of the fused ligand (**LAf**) as a result of its intrinsic structural rigidity.

This small structural difference could determine a difference in stability of the two systems at the ground state and could also possibly affect the photostability of the complex **PAf**.

Concerning the geometrical decoupling between the photosensitizer and the acceptor unit, it is clear that it is minimized (and the electronic coupling maximized) by the perfect coplanarity of the **LAf** ligand within the **PAf** dyad, contrarily to the case of **P-Ab**. In the latter case, a significant geometrical decoupling is indeed computed between

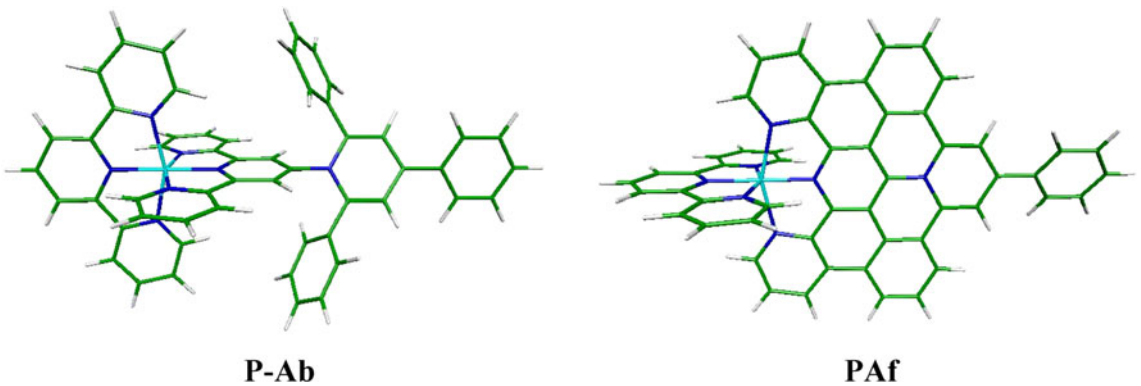

Fig. 2 Optimized ground state structures obtained for **P-Ab** and **PAf** in the gas phase

the planes of the tpy and of the pyridinium, which amounts to ca. 68.4°, in qualitative agreement with the X-ray structural data ($\theta_{\text{a-Xray}} = 79.38°$) [37].

Beyond these structural differences, the electronic structures of both complexes **P-Ab** and **PAf** are qualitatively very similar. The HOMOs correspond to three degenerate molecular orbitals with the larger contribution of the d orbitals centered on the Ru atom, in agreement with the electronic structure expected for a d^6 metal in a (pseudo)octahedral environment. The LUMOs, on the other hand, display important contributions from orbitals centered on the ligand carrying the acceptor (pyridinium core). Indeed, if in the case of **P-Ab** the LUMO is still mostly centered on the tpy part (Figure SI.3), in the case of **PAf**, a substantial contribution from the pyridinium core is pointed out (Figure SI.3) although the orbitals look much delocalized over the π-conjugated framework. This finding is consistent with the geometrical decoupling of the acceptor unit observed in the case of **P-Ab**.

Going from **P-Ab** to **PAf** also corresponds to a significant lowering of the LUMO energy, and thus to a reduction in the gap (of ca. 0.3 eV) and to a densification of electronic excited states. Therefore, a sizable shift to lower energies is expected in the spectral features of fused complex as compared to the branched analogs.

4 Electronic structures and optical properties

The electronic transitions associated with the branched (**L-Ab**) and fused (**LAf**) ligands (depicted in Fig. 1), computed in the gas phase using a TD-DFT approach, are collected in Table 3 and depicted in Fig. 3, in comparison with the available experimental spectrum of **L-Ab** recorded in CH_3CN.

Since the main effect of the presence of a phenyl substituent at the position 4 of the pyridinium ring is just an increase in the intensity associated with the most relevant electronic transitions with respect to the corresponding hydrogenated compounds (**L-Ab^{H}** and **LAf^{H}**), the spectral features of these latter are only reported in Supporting Information (Table SI.3). Data corresponding to the parent acceptors (**Ab** and **Af**) computed in the gas phase are also reported in Supporting Information (Table SI.4).

From the analysis of Fig. 3, it clearly appears as a striking feature that the cyclization (i.e., fusion) of **L-Ab** is resulting in an extended absorption spectrum toward lower energies for the **LAf** ligand. Besides, as regards the fused species, the computed densification of the excited states in the energy range close to the HOMO–LUMO gap gives rise to an absorption spectrum showing an overall complex spectral pattern in the UV–visible region. Therefore, if the

Table 3 Principal computed electronic transitions (in nm) with associated oscillator strength (*f*, in a.u.) in parenthesis

	λ_{max} (f)									
L-Ab	332	329	323.5	311	292	271	268			
	(0.19)	(0.15)	(0.12)	(0.49)	(0.13)	(0.12)	(0.29)			
LAf	444	418	366	365	340	332	292	291	287	275
	(0.08)	(0.05)	(0.08)	(0.16)	(0.64)	(0.19)	(0.11)	(0.15)	(0.32)	(0.54)
LAf	420	385	349	340	337	330	312	290	284	280
(in CH_3CN)	(0.21)	(0.09)	(0.45)	(0.02)	(0.63)	(0.66)	(0.08)	(0.16)	(0.16)	(0.57)

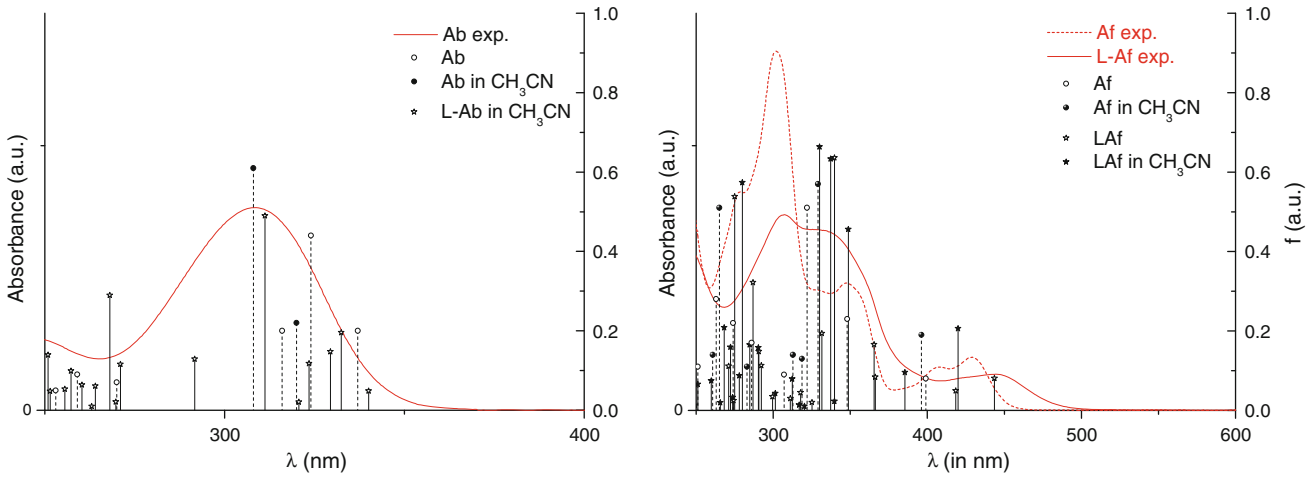

Fig. 3 Computed and experimental spectra of branched and fused acceptors and ligands

electronic spectra of branched pyridiniums are constituted by a simple spectral pattern, the fused species **Af** and **LAf** present complex spectral features, displaying several transitions in the UV–visible region. This prediction is fully consistent with the experimental spectra available not only for **Af** but also for the peculiar *hemi*-fused derivative of **L-Ab** hereafter referred to as **L-Af**, whose schematic structure is given in Fig. 4 (see also Sect. 5).

Let us focus first on the electronic transitions computed for the **L-Ab** branched ligand. This system shows four transitions at energy lower than 4.13 eV, that is, corresponding to wavelengths larger than 300 nm: the most intense being computed at 311 nm, responsible for the dominant band indeed experimentally observed for this species around 310 nm. Whether concerning their energy or their nature, these transitions are closely akin to the transitions computed for the acceptor **Ab**, thereby further substantiating a significant electronic decoupling between the tpy and acceptor unit within **L-Ab**.

All transitions show an intramolecular charge-transfer (ICT) character from phenyl groups (at positions 2, 6 and 4) toward the central pyridinium platform, where the LUMO is centered (Supporting Information, Figure SI.2).

The transitions computed at higher energies have mainly a π–π^* character, and they are centered on the tpy. Of note, also, is the observation that transitions showing a partial CT character from the tpy to the pyridinium ring are computed in the same spectral region, but with lower intensity due to the significant structural/electronic decoupling of the two moieties. Finally, at even higher energies (around 235 nm), π–π^* transitions involving only orbitals belonging to the pyridinium core are computed. Therefore, from the spectral data computed for the **L-Ab** ligand, it seems clear that in spite of the computed decoupling of the tpy and pyridinium moieties, which allows to interpreting the spectral properties of the ligand as being essentially the sum of the spectral features of its isolated components, there exists some residual coupling between the tpy to the pyridinium subunits.

The analysis of the vertical transitions computed for the—fully—fused ligand (**LAf**) provides with a completely different picture of the electronic landscape. All transitions occurring in the UV–vis. region are of π–π^* type with no significant ICT character, in agreement with findings previously reported in a detailed analysis of the spectral properties of the isolated acceptor [24, 26].

Indeed, for **LAf** the first noticeable transitions (computed at 444, 418, 366 and 365 nm) correspond to excitations from orbitals centered on the tpy fragment of the fused polycyclic moiety to the LUMO, which presents a larger contribution on the pyridinium core. These transitions are also significantly shifted with respect to those of the parent acceptor (**Af**), thereby clearly indicating that the fusion by cyclization with the tpy moiety strongly affects the electronic properties of the whole system, contrary to what was found in the case of the branched analog. This behavior is consistent with the bathochromic shift of the first band (low-energy edge) experimentally observed when going from the fused acceptor **Af** to the *hemi*-fused ligand **L-Af** (Fig. 4), as shown in Fig. 3.

As already discussed in previous works concerning the isolated fused acceptor **Af**, the structure observed for the first band is mainly ascribable to vibronic effects related to the torsional motion of the terminal phenyl ring [24]. Finally, inclusion of solvent effects in the case of the fused ligand (Fig. 3) only slightly shifts the first (lower energy) absorption band, leaving the overall spectral features unchanged, as expected on the basis of the poor (I)CT character of these electronic transitions.

As regards the affiliated dyads whose computed transitions are reported in Fig. 5 and listed in Table 4, it is clear that going from the branched complex to the fused compound is accompanied with a significant red-shift of the first absorption band. More precisely, the computed energy corresponding to the first excited state is shifted by roughly 0.38 eV toward the visible spectral region when moving from **P-Ab** to **PAf**. The same trend is observed in the case of the **P-Ab^{H}** and **PAf^{H}** whose computed transitions are

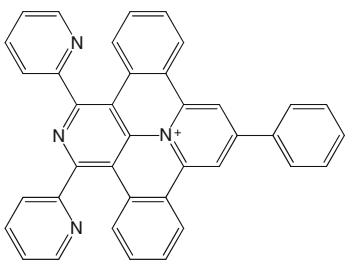

L-Af

Fig. 4 The hemi-fused ligand **L-Af**

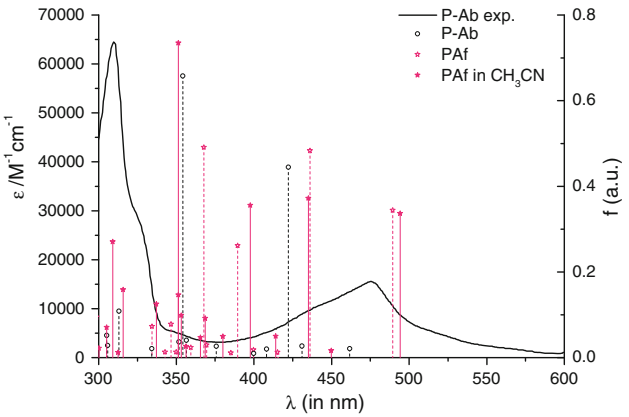

Fig. 5 Computed spectra of **P-Ab** and **PAf** together with the experimental spectra of **P-Ab** recorded in CH_3CN

Table 4 Electronic transitions (in nm) and associated oscillator strengths (a.u., in parenthesis) computed for **P-Ab** and **PAf**

	λ_{max} (f)							
P-Ab	461	430	423	408	375	356	354	
	(0.02)	(0.03)	(0.44)	(0.02)	(0.03)	(0.04)	(0.65)	
PAf	489	436	415	400	389	369	367	359
	(0.34)	(0.48)	(0.01)	(0.02)	(0.26)	(0.03)	(0.49)	(0.02)
PAf	494	448	433	414	397	380	369	363
(in CH_3CN)	(0.20)	(0.02)	(0.30)	(0.05)	(0.39)	(0.05)	(0.09)	(0.04)

practically isoenergetic to those calculated for **P-Ab** and **PAf**, the only difference being related to their intensity (Supporting Information, Figure SI.4).

On scrutinizing the spectrum of the branched compound (**P-Ab**), it can be noted that the lowest lying transitions are of MLCT nature with no significant contribution from orbitals centered on the acceptor unit. This means that these transitions have a very limited CT character, in line with expectations related to the above-established structural and electronic decoupling between the photosensitizer and the electron-withdrawing unit.

On the other hand, transitions of significant intensity computed at higher energies (around 350 nm) have a ligand-centered (LC) character. The most intense among them is fully centered on the acceptor unit and corresponds to a CT from the phenyl substituents to pyridinium core. Overall, the computed transitions are consistent with the experimental spectrum recorded for **P-Ab**, excepted for a systematic ipsochromic shift, which is mainly ascribable to the neglecting of solvent effects.

In the case of the fused complex (**PAf**), the computed spectrum shows several intense transitions in the visible range, which are all of MLCT character. In this case, the virtual orbitals involved are delocalized over the whole π-conjugated system including the pyridinium ring.[1] On the bases of both the large number of transitions computed and their very close energy, the effect of the presence of a "large-surface" ligand such as **LAf** in the coordination compound **PAf** is therefore twofold: (i) a great enhancement of the absorption properties of the complex (improved absorption cross-section) and (ii) an extension of the red-edge absorption toward the visible region (shift to lower energy of the first—lower energy—band). In other words, this complex **PAf** represents a step forward toward a black absorber as compared to the parent—branched—analog **P-Ab**.

5 Discussion and conclusions

From the computational picture that we get of the electronic features of **PAf** as compared to the non-fused analog **P-Ab**, it appears that the former coordination compound is worthwhile to be synthesized. The synthetic strategy initially envisaged to obtain the "large-surface" ligand **LAf** was adapted from the photochemical route normally used to form fused polycyclic expanded pyridiniums of type **Af** [25, 27, 1, 40–42]. This approach is based on the photobiscyclization reaction originally developed by Katritzky and coworkers [43, 44]. Unfortunately, the first attempts to synthesize **LAf** from **L-Ab** remained unsuccessful. Instead of yielding to the fully fused target ligand, the photoinduced cyclodehydrogenation of **L-Ab** resulted in the hemi-fused photoproduct, **L-Af** (see Figs. 4, 6 as well as Supporting Information for other characterizations). Moreover, this species was formed with a very low yield of a few percents. This low yield can be explained by the highly constraint nature of the molecular skeleton of the hemi-fused ligand (**L-Af**), which is clearly evidenced by the single-crystal X-ray analysis (Fig. 6).[2] Besides, this intramolecular steric hindrance not only precludes further cyclodehydrogenation toward the fully fused ligand (**LAf**) but also locks the tpy fragment in a conformation improper to coordination with a d^6 transition metal like ruthenium(II).

Alternative synthetic strategies are currently underway to overcome the above-mentioned problem and to obtain the target "large-surface" ligand, **LAf**.

Indeed, from insights collected at the theoretical level, it is clear that the design strategy here adopted and aimed at targeting condensed electron-acceptors as ligands (namely derivatives of fused expanded pyridiniums) seems to be adapted to obtain a densification of electronic states with a concomitant red-shift and enhancement of the absorption in the visible range while leaving the frontier orbitals character unchanged. These peculiar features are thus consistent

[1] In the case of **PAf**, solvent effects were considered but found to be negligible since they only slightly shift the maxima computed in the gas phase, in agreement with the delocalized π nature of the virtual orbitals involved in the MLCT transitions, which are indeed expected to be less solvatochromic than truly CT excitations.

[2] CCDC-831781 ([**L-Af**]$(BF_4)\cdot CH_3CN$) contains the supplementary crystallographic data for this paper. These data can be obtained free of charge from The Cambridge Crystallographic Data Centre via http://www.ccdc.cam.ac.uk/data_request/cif.

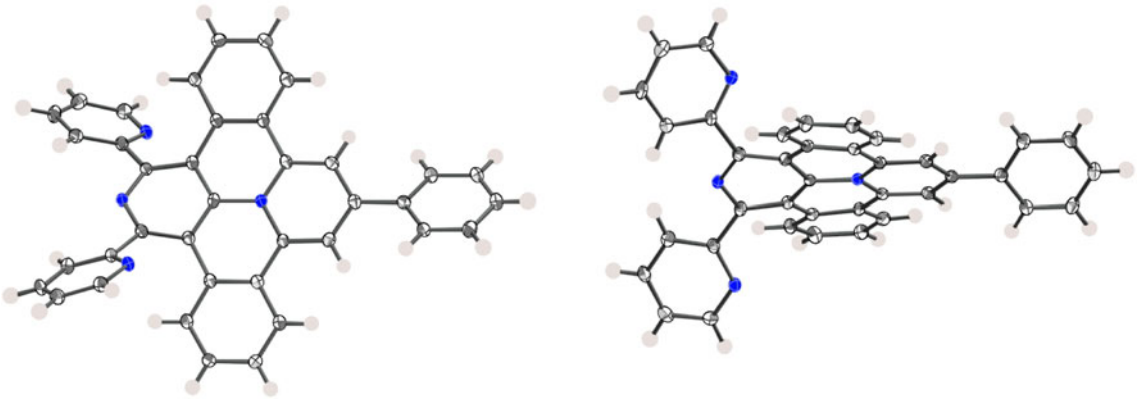

Fig. 6 X-ray structure: Ortep drawings of the molecular entity (*top* and *side views*). The co-crystallized solvent molecule (MeCN) and the counter-anion (BF_4^-) have been omitted for clarity

with their use as panchromatic dyes, for instance, for DSSCs applications.

Acknowledgments The ANR is gratefully acknowledged for financial support in the framework of the NEXUS project (Programme Blanc 2007, BLAN07-1-196405). Dr Jérôme Fortage is acknowledged for fruitful discussions.

References

1. Balzani V, Credi A, Venturi M (2009) Chem Soc Rev 38: 1542–1550
2. Lainé PP, Campagna S, Loiseau F (2008) Coord Chem Rev 252:2552–2571
3. Juris A, Balzani V, Barigelletti F, Campagna S, Belser P, Von Zelewsky A (1988) Coord Chem Rev 84:85–277
4. Anderson PA, Keene FR, Meyer TJ, Moss JA, Strouse GF, Treadway JA (2002) J Chem Soc Dalton Trans 3820–3831
5. Nazeeruddin MdK, Péchy P, Renouard T, Zakeeruddin SM, Humphry-Baker R, Comte P, Liska P, Cevey L, Costa E, Shklover V, Spiccia L, Deacon GB, Bignozzi CA, Grätzel M (2001) J Am Chem Soc 123:1613–1624
6. Browne WR, O'Boyle NM, McGarvey JJ, Vos JG (2005) Chem Soc Rev 34:641–663
7. Balzani V, Juris A, Venturi M, Campagna S, Serroni S (1996) Chem Rev 96:759–833
8. Herrera JM, Pope SJA, Meijer AJHM, Easun TL, Adams H, Alsindi WZ, Sun XZ, George MW, Faulkner S, Ward MD (2007) J Am Chem Soc 129:11491–11504
9. Glazer EC, Tor Y (2002) Angew Chem Int Ed 41:4022–4026
10. Draper SM, Gregg DJ, Schofield ER, Browne WR, Duati M, Vos JG, Passaniti P (2004) J Am Chem Soc 126:8694–8701
11. Draper SM, Gregg DJ, Madathil R (2002) J Am Chem Soc 124:3486–3487
12. Gregg DJ, Bothe E, Holfer P, Passaniti P, Draper SM (2005) Inorg Chem 44:5654–5660
13. Lainé PP, Bedioui F, Loiseau F, Chiorboli C, Campagna S (2006) J Am Chem Soc 128:7510–7521
14. Lainé PP, Loiseau F, Campagna S, Ciofini I, Adamo C (2006) Inorg Chem 45:5538–5551
15. Lainé PP, Ciofini I, Ochsenbein P, Amouyal E, Adamo C, Bedioui F (2005) Chem Eur J 11:3711–3727
16. Ciofini I, Lainé PP, Bedioui F, Adamo C (2004) J Am Chem Soc 126:10763–10777
17. Abbotto A, Sauvage F, Barolo C, De Angelis F, Fantacci S, Graetzel M, Manfredi N, Marinzi C, Nazeeruddin MK (2011) Dalton Trans 40:234–242
18. De Angelis F, Fantacci S, Selloni A, Nazeeruddin MK, Gratzel M (2010) J Phys Chem C 114:6054–6061
19. Lobello MG, Fantacci S, Credi A, De Angelis F (2011) Eur J Inorg Chem 10:1605–1613
20. Nazeeruddin MK, Bessho T, Cevey L, Ito S, Klein C, De Angelis F, Fantacci S, Comte P, Liska P, Imai H, Graetzel M (2007) J Photochem Photobiol A Chemistry 185:331–337
21. Tachibana Y, Moser JE, Grätzel M, Klug DR, Durrant JR (1996) J Phys Chem 100:20056–20062
22. Brennaman MK, Alstrum-Acevedo JH, Fleming CN, Jang P, Meyer TJ, Papanikolas JM (2002) J Am Chem Soc 124: 15094–15098
23. Chiorboli C, Rodgers MAJ, Scandola F (2003) J Am Chem Soc 125:483–491
24. Peltier C, Lainé PP, Scalmani G, Frisch MJ, Adamo C, Ciofini I (2009) J Mol Struct THEOCHEM 914:94–99
25. Fortage J, Tuyèras F, Ochsenbein P, Puntoriero F, Nastasi F, Campagna S, Griveau S, Bedioui F, Ciofini I, Lainé PP (2010) Chem Eur J 16:11047–11063
26. Peltier C, Adamo C, Lainé PP, Campagna S, Puntoriero F, Ciofini I (2010) J Phys Chem A 114:8434–8443
27. Fortage J, Peltier C, Nastasi F, Puntoriero F, Tuyèras F, Griveau S, Bedioui F, Adamo C, Ciofini I, Campagna S, Lainé PP (2010) J Am Chem Soc 132:16700–16713
28. Vlček A, Záliš S (2007) Coord Chem Rev 251:258–267
29. Jacquemin D, Perpete EA, Ciofini I, Adamo C (2009) Acc Chem Res 42:326–334
30. Dreuw A, Head-Gordon M (2004) J Am Chem Soc 126:4007–4016
31. Le Bahers T, Adamo C, Ciofini I (2011) JCTC 7:2498–2506
32. Peach MJG, Benfield P, Helgaker T, Tozer DJ (2008) J Chem Phys 128:044118
33. Frisch MJ et al (2010) Gaussian 09, Revision A.02, Gaussian, Inc., Wallingford CT
34. Adamo C, Barone V (1999) J Chem Phys 110:6158
35. Tomasi J, Mennucci B, Cammi R (2005) Chem Rev 105:2999–3094
36. Barone V, Cossi M (1998) J Phys Chem A 102:1995–2001
37. Lainé P, Bedioui F, Ochsenbein P, Marvaud V, Bonin M, Amouyal E (2002) J Am Chem Soc 124:1364–1377
38. Lainé P, Bedioui F, Amouyal E, Albin V, Berruyer-Penaud F (2002) Chem Eur J 8:3162–3176
39. Lainé P, Amouyal E (1999) Chem Commun 935–936

40. Le Bahers T, Labat F, Pauporté T, Lainé PP, Ciofini I (2011) J Am Chem Soc 133:8005–8013
41. Wu D, Pisula W, Enkelmann V, Feng X, Müllen K (2009) J Am Chem Soc 131:9620–9621
42. Wu D, Zhi L, Bodwell GJ, Cui G, Tsao N, Müllen K (2007) Angew Chem Int Ed 46:5417–5420
43. Katritzky AR, Zakaria Z, Lunt E, Jones PG, Kennard O (1979) J Chem Soc Chem Commun 268–269
44. Katritzky AR, Zakaria Z, Lunt E (1980) J Chem Soc Perkin Trans 1:1879–1887